A Simple Method Relating Specific Rate Constants $k(E,J)$ and Thermally Averaged Rate Constants $k_\infty(T)$ of Unimolecular Bond Fission and the Reverse Barrierless Association Reactions†

J. Troe*,‡ and V. G. Ushakov‡,§

Institut for Physical Chemistry, University of Göttingen, Tammannstrasse 6, D-37077 Göttingen, Germany, and Institute of Problems of Chemical Physics, Russian Academy of Sciences, 142432 Chernogolovka, Russia

Received: October 31, 2005; In Final Form: December 6, 2005

This work describes a simple method linking specific rate constants $k(E,J)$ of bond fission reactions AB → A + B with thermally averaged capture rate constants $k_{cap}(T)$ of the reverse barrierless combination reactions A + B → AB (or the corresponding high-pressure dissociation or recombination rate constants $k_\infty(T)$). Practical applications are given for ionic and neutral reaction systems. The method, in the first stage, requires a phase-space theoretical treatment with the most realistic minimum energy path potential available, either from reduced dimensionality ab initio or from model calculations of the potential, providing the centrifugal barriers $E_0(J)$. The effects of the anisotropy of the potential afterward are expressed in terms of specific and thermal rigidity factors $f_{rigid}(E,J)$ and $f_{rigid}(T)$, respectively. Simple relationships provide a link between $f_{rigid}(E,\langle J\rangle)$ and $f_{rigid}(T)$ where $\langle J\rangle$ is an average value of J related to $J_{max}(E)$, i.e., the maximum J value compatible with $E \geq E_0(J)$, and $f_{rigid}(E,\langle J\rangle)$ applies to the transitional modes. Methods for constructing $f_{rigid}(E,J)$ from $f_{rigid}(E,\langle J\rangle)$ are also described. The derived relationships are adaptable and can be used on that level of information which is available either from more detailed theoretical calculations or from limited experimental information on specific or thermally averaged rate constants. The examples used for illustration are the systems $C_6H_6^+ \leftrightarrow C_6H_5^+ + H$, $C_8H_{10}^+ \rightarrow C_7H_7^+ + CH_3$, $n\text{-}C_9H_{12}^+ \leftrightarrow C_7H_7^+ + C_2H_5$, $n\text{-}C_{10}H_{14}^+ \leftrightarrow C_7H_7^+ + C_3H_7$, $HO_2 \leftrightarrow H + O_2$, $HO_2 \leftrightarrow HO + O$, and $H_2O_2 \leftrightarrow 2HO$.

1. Introduction

Sophisticated experimental and theoretical techniques over the past decades have been developed which allow to study state-resolved unimolecular reaction dynamics on a very detailed level; for instance, see ref 1. The transformation of the derived quantities into and the comparison with thermally averaged quantities may look like a trivial task. However the contrary is the case. Each of the derived quantities in general is sensitive to different properties of the reaction system such that state-specific and thermally averaged measurements in most cases are complementary. Obviously, they should be linked in an intrinsically consistent way. It is the aim of the present article to provide a simple approximate method which is suitable for this purpose.

There are various ways to link state-specific and thermally averaged quantities. For instance, one may have a complete potential energy surface of the system from ab initio calculations and perform dynamical, either quantum or classical, calculations on them. Then a correct relation between state-specific and thermally averaged quantities is directly accessible. In practice, unfortunately one is far from this situation, theoretical as well as experimental information being only fragmentary. Our work addresses this case. On the theoretical side, we rely on statistical adiabatic channel model/classical trajectory (SACM/CT) calculations such as performed in refs 2−6. This approach employs reduced dimensionality potential energy surfaces for transitional modes, constructed either from ab initio or from model calculations. On the experimental side, we rely either on measurements of specific rate constants $k(E)$ for dissociation over certain energy ranges or on measurements of rate constants $k_{cap}(T)$ for capture (or association, recombination, and the reverse dissociation) over certain temperature ranges. The method can be applied with or without detailed SACM/CT results and can be adapted to the amount of available information. It applies to ionic as well as neutral reaction systems and illustrative examples are given for both classes of reactions.

2. General Formalism

Our approach is based on an SACM/CT treatment where conserved and transitional modes are separated such that reduced dimensionality potentials can be employed. We consider the process

$$A + B \leftrightarrow AB \tag{2.1}$$

and, for simplicity, identify the conserved modes with the internal modes of A and B, excluding their external rotations. Our goal is to relate specific rate constants $k(E,J)$ for dissociation of AB with thermally averaged rate constants for dissociation of AB or, more conveniently, with thermal high-pressure rate constants $k_{rec,\infty}(T)$ for recombination of A and B. Omitting electronic partition functions Q_{el} from $k_{rec,\infty}(T)$, we focus attention on thermal capture rate constants $k_{cap}(T)$, related to $k_{rec,\infty}(T)$ by

$$k_{rec\infty}(T) = [Q_{el,AB}/Q_{el,A}Q_{el,B}]\, k_{cap}(T) \tag{2.2}$$

† Part of the special issue "David M. Golden Festschrift".

* Corresponding author. E-mail: shoff@gwdg.de

‡ University of Göttingen.

§ Russian Academy of Sciences.

10.1021/jp056269s CCC: $33.50
Published on Web 01/20/2006

In detail, $k_{cap}(T)$ is given by[1,7]

$$k_{cap}(T) = \frac{kT}{hQ_{tr}Q_AQ_B}\int_0^\infty \sum_J (2J+1)W(E,J)\exp\left(-\frac{E}{kT}\right)\frac{dE}{kT} \quad (2.3)$$

where Q_{tr} is the product of translational partition functions

$$Q_{tr} = (2\pi\mu kT/h^2)^{3/2} \quad (2.4)$$

with the reduced mass μ of the reaction pair A and B. $W(E,J)$ denotes the number of "activated complex states" or "open channels", or the "cumulative reaction probability"[1]. Q_A and Q_B are rovibrational partition functions of A and B, respectively. At the same level, specific rate constants $k(E,J)$ are expressed by

$$k(E,J) = W(E,J)/h\rho(E,J) \quad (2.5)$$

with the rovibrational density of states $\rho(E,J)$ of AB. E is the total rovibrational energy of the system and the total angular momentum is characterized by its quantum number J.

2.1. Phase Space Theory. The present approach intends to be as general as possible. This means that it has to be designed as close to the real potential energy surface (PES) as possible. However, it restricts attention to a reduced dimensionality PES for the transitional modes which has the advantage that molecular systems of arbitrary size can be handled with equal effort. It avoids the guess of more or less undefined "activated complex frequencies" which are often used as fit parameters in the Rice−Ramsperger−Kassel−Marcus (RRKM) theory. On the way to a relation between $k(E,J)$ and $k_{cap}(T)$, which is the goal of the present article, it is obligatory to construct the most realistic phase space theory (PST) possible. PST neglects the anisotropy of the interaction of the potential between A and B. PSTs have been constructed on different levels,[1] without any centrifugal barriers $E_0(J)$, with centrifugal barriers such as calculated from the long-range part of the interaction between A and B only (orbiting transition state theory, OTS), and with centrifugal barriers determined from the complete short-range/long-range PES and its minimum energy path (MEP) obtained from ab initio or model PESs. We are convinced that only the latter version of PST can be of general use, treating neutral and ionic reaction systems on a common ground. This does not mean that simpler versions of PST cannot be realistic under some circumstances.

Q_A, Q_B, $W(E,J)$, and $\rho(E,J)$ in eqs 2.3 and 2.5 contain contributions from conserved and transitional modes. Within the present SACM/CT approach, these are separable such that the contributions from conserved modes in the integral over $W(E,J)$ in eq 2.3 cancel against the contributions in Q_A and Q_B. As a result, only contributions from transitional modes need to be considered in $W(E,J)$, Q_A, and Q_B in eq 2.3. The situation is slightly more complicated for $k(E,J)$ in eq 2.5 where one has to include contributions from conserved modes of A and B and transitional modes in $W(E,J)$, while $\rho(E,J)$ is determined by the modes of AB. The contributions from the conserved modes, therefore, cannot be factored out and canceled such as in the thermal rate constants given by eq 2.3.

On the basis of the previous thoughts, in the following we first elaborate a PST for $k_{cap}(T)$. Within the integral of eq 2.3 the summation over $W(E,J)$ can either go over J from 0 to J_{max}, or $W(E,J)$ is replaced by $W(E,L)$ and L summed from 0 to L_{max}. Here L denotes the quantum number of the orbital angular momentum of the relative motion of A and B. The maximum values J_{max} or L_{max} define the range of J or L in which centrifugal barriers $E_0(J)$ and $E_0(L)$ can be overcome on the way from A and B to AB, i.e., in which $E \geq E_0(J)$ or $E \geq E_0(L)$. E_0(J) and E_0(L) are not identical, see ref 2. However, J approaches L for large values of both quantities which are most relevant in thermal recombination experiments. Likewise, most experimental studies of $k(E)$ have been done under conditions of comparably large J such that $J \approx L$ represents an adequate approximation.

We write $W(E,L)$ in the form

$$W(E,L) = W(E - E_0(L)) = W(z) \quad (2.6)$$

with

$$z = E - E_0(L) \quad (2.7)$$

where $W(z)$ is equal to the number of quantum states of the combined system A + B in the energy range 0 to z. The integral in eq 2.3 can be executed with the result

$$\int_0^\infty W(z)\exp(-z/kT)\,dz/kT = Q_AQ_B \quad (2.8)$$

such that eq 2.3 reads

$$k_{cap}^{PST}(T) = \frac{kT}{hQ_{tr}}\sum_L (2L+1)\exp[-E_0(L)/kT] \quad (2.9)$$

Elaborating the relationship between the centrifugal barriers $E_0(L)$ and the PES then leads to well-known expressions for k_{cap}^{PST}, for instance to the Langevin equation $k_{cap}^{PST} = k_L = 2\pi q\sqrt{\alpha/\mu}$ for ion-induced dipole PESs (q = ionic charge of A, α = polarizability of B), or to locked-dipole theory for ion-permanent dipole PESs $k_{cap}^{PST} = k_{LD} = 2\pi q\mu_D\sqrt{2/\pi\mu kT}$ (μ_D = dipole moment of B). PSTs for valence potentials (Gorin models or loose transition state theory employing realistic MEPs of the potential) can be handled in the same way as well.

The situation is more complicated for a PST treatment of $k(E,J)$. Here, as mentioned above, the convolution over conserved and transitional modes, for instance in a Beyer−Swinehart/Stein−Rabinovitch state counting routine for $W(E,J)$ (see refs 8 and 9), can hardly be avoided. Considering the transitional mode part only, which in the following exclusively is included in $W(E,J)$, there are practically useful expressions available (see refs 10−13) for all types of molecular complexities (A + B = atom + linear, atom + spherical top, linear + linear, linear + spherical top, spherical top + spherical top). However, these expressions only apply to PST without centrifugal barriers, i.e., with $E_0(J) \approx E_0(L) \approx 0$. Denoting the corresponding $W(E,J)$ by $W_0(E,J)$, fortunately, we found a way to approximately account for the true centrifugal barriers: SACM/CT calculations in refs 2 and 5 showed that, for large $J \approx L$

$$W^{PST}(E,J) = W_0(E,J)\,w(E,J) \quad (2.10)$$

with a PST-capture probability $w(E,J)$ given by

$$w(E,J) \approx [1 - E_0(J)/E]^n \quad (2.11)$$

The exponent n is equal to 1, 1.5, 2, 2.5, and 3 for atom + linear, atom + spherical top, linear + linear, linear + spherical top, and spherical top + spherical top combinations of A + B, respectively. This solves the problem of calculating $W(E,J)$ in PST. The second task of determining $\rho(E,J)$ is not trivial. Apart

from the J dependence of $\rho(E,J)$, see refs 11−15, there is the problem of anharmonicity contributions which is far from being solved. Leaving these complications aside, however, the given expressions for $W(E,J)$, together with $\rho(E,J)$, provide a direct and simple link between $k(E,J)$ and $k_{cap}(T)$ within the framework of PST.

2.2. Results for Anisotropic Potentials. The real complication of the problem comes in through the anisotropy of the PES which reduces $k_{cap}(T)$ and $k(E,J)$ to values below those given by PST. In reality, all potentials are more or less anisotropic and even PESs, which are isotropic at large A−B distances, at small A−B distances contain considerable and often underestimated anisotropic components arising from short-range valence contributions to the PES. We characterize these anisotropy effects by rigidity factors f_{rigid}, defined by

$$k_{cap}(T) = f_{rigid}(T) k_{cap}{}^{PST}(T) \tag{2.12}$$

and

$$W(E,J) = f_{rigid}(E,J)\, W^{PST}(E,J) \tag{2.13}$$

where $f_{rigid}(E,J)$ and $W^{PST}(E,J)$ correspond to the transitional modes only. The convolution of the contributions from transitional and conserved modes leads to the total $W(E,J)$ employed in the calculation of the specific rate constants $k(E,J)$ in eqs 2.3 and 2.5 as well as in section 2.1.

Our full SACM/CT treatments of the processes of eq 2.1, both on ab initio and on model PESs, have given detailed results for $f_{rigid}(T)$ and $f_{rigid}(E,J)$; see refs 2−6. These trajectory calculations may appear routine today. They are nevertheless time consuming, and it is the aim of the present article to provide short-cuts and avoid the CT-calculations.

In what follows, we neglect the difference between J and L. We inspect the results of SACM/CT from refs 2−6 and first consider the case when $f_{rigid}(E,J)$ is of the form

$$f_{rigid}(E,J) \approx f_{rigid}(E - E_0(J)) = f_{rigid}(z) \tag{2.14}$$

where z as above is given by $z = E - E_0(J)$. In general, there will be a complicated J dependence of $f_{rigid}(E,J)$ in addition to that through $E - E_0(J)$. We shall show examples of such dependences below. However, detailed calculations of $f_{rigid}(E,J)$ show that the J-dependent curves sometimes can approximately be collapsed into one curve $f_{rigid}(z)$ such as illustrated below. Figure 1 gives an example from ref 5 for the reaction system $C_8H_{10}^+ \leftrightarrow C_7H_7^+ + CH_3$ which will be considered in more detail below. Cases like this are particularly simple to handle such as demonstrated in the following sentences.

If eq 2.14 is valid, one may insert eqs 2.6 and 2.14 into eq 2.3 and obtain

$$k_{cap}(T) \approx \frac{kT}{hQ_{tr}Q_AQ_B}\sum_J (2J+1) \exp[-E_0(J)/kT]\int_0^\infty f_{rigid}(z)W(z)\exp(-z/kT)\,dz/kT \tag{2.15}$$

If the specific rigidity factor for the transitional modes $f_{rigid}(E,J)$ from eq 2.14 now can be represented in exponential form

$$f_{rigid}(z) \approx \exp(-z/kT_0) \tag{2.16}$$

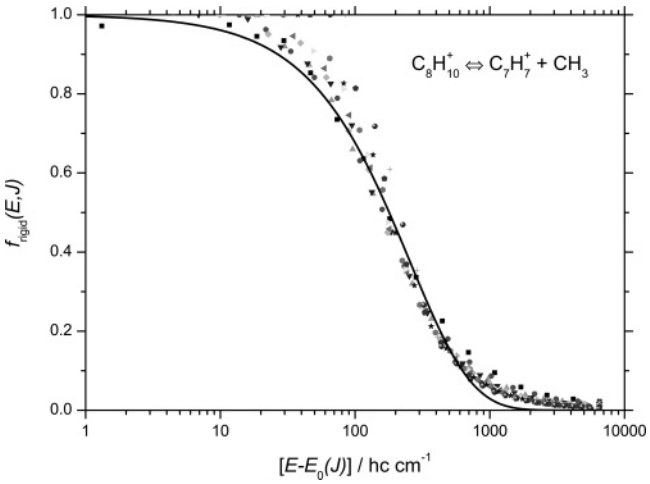

Figure 1. Specific rigidity factors $f_{rigid}(E,J)$ for the transitional modes in the dissociation of ethylbenzene cations $C_8H_{10}^+ \leftrightarrow C_7H_7^+$ (benzylium) + CH_3 (points, SACM/CT calculations[5] for individual J in the range 25−210 with $E_0(J)$/hc in the range 0.82−750 cm^{-1}; for symbols, see ref 5; full line, empirical representation by $f_{rigid}(E,J) \approx \exp\{-[E - E_0(J)]/kT_0\}$ with the empirical fit parameter $T_0 = 376$ K).

with an empirical fit parameter T_0, then the integral in eq 2.15 can be solved, giving

$$\int_0^\infty f_{rigid}(z)W(z)\exp(-z/kT)\,dz/kT \approx (\tau/T)Q_A(\tau)Q_B(\tau) \tag{2.17}$$

with

$$\tau = T_0T/(T_0 + T) \tag{2.18}$$

This leads to

$$k_{cap}(T) \approx \left(\frac{\tau}{T}\right)\frac{Q_A(\tau)Q_B(\tau)}{Q_A(T)Q_B(T)}k_{cap}{}^{PST}(T) \tag{2.19}$$

As a consequence we finally obtain

$$k_{cap}(T) \approx (\tau/T)^n k_{cap}{}^{PST}(T) \tag{2.20}$$

with $n = 2$, 2.5, 3, 3.5, and 4 for A + B = atom + linear, atom + spherical top, linear + linear, linear + spherical top, and spherical top + spherical top combinations, respectively. For this special case, we have thus established a simple relationship between specific rigidity factors for the transitional modes of the form $f_{rigid}(E,J) \approx f_{rigid}(z) = \exp(-z/kT_0)$, with $z = E - E_0(J)$ from eq 2.16 and the empirical fit parameter T_0, and thermal rigidity factors

$$f_{rigid}(T) \approx (\tau/T)^n \tag{2.21}$$

in eq 2.20.

In the same way as before one may generalize eq 2.16 for the case that specific rigidity factors can be approximated by

$$f_{rigid}(z) \approx f_0 + f_1\exp(-z/kT_1) + f_2\exp(-z/kT_2) + ... \tag{2.22}$$

In this case, we derive

$$k_{cap}(T) \approx [f_0 + f_1(\tau_1/T)^n + f_2(\tau_2/T)^n + ...]\, k_{cap}{}^{PST}(T) \tag{2.23}$$

This gives

$$f_{\text{rigid}}(T) \approx f_0 + f_1(\tau_1/T)^n + f_2(\tau_2/T)^n + ... \quad (2.24)$$

where the exponent n is defined as in eq 2.20 and

$$\tau_i = T_i T/(T_i + T) \quad (2.25)$$

We have again established a relationship between the specific rigidity factors from eq 2.22, with the empirical fit parameters f_i and T_i and thermal rigidity factors given by eq 2.24. The fits can be used in either direction, from $f_{\text{rigid}}(z)$ to $f_{\text{rigid}}(T)$ or vice versa. The following section demonstrates how this simple procedure, which short-cuts the cumbersome complete SACM/CT calculations, can be exploited in practice.

If $f_{\text{rigid}}(E,J)$ has a more complicated J dependence than given by eq 2.14, one can obviously not conclude from $f_{\text{rigid}}(T)$ on the detailed E and J dependences of $f_{\text{rigid}}(E,J)$. Instead, one can only derive $f_{\text{rigid}}(E,\langle J\rangle)$ for an average J and ask for the meaning of the corresponding average value $\langle J\rangle$ of the angular momentum quantum number J. This question may look difficult to answer in general. However, our detailed SACM/CT calculations from refs 2−6 provide relationships between $\langle J\rangle$ and J_{max} which can be used for practical applications. SACM/CT calculations of $f_{\text{rigid}}(E,J)$ and $f_{\text{rigid}}(T)$, for a variety of model potentials, in ref 2 showed that indeed $\langle J\rangle$ is linked to J_{max}. For instance, for ion-permanent dipole potentials with $E_0(J) = 0$ for $J \le J_{\text{max}}$, we derived[2]

$$f_{\text{rigid}}(T) \approx 0.5 \quad (2.26)$$

and

$$f_{\text{rigid}}(E,J) \approx 1 - (J/J_{\text{max}})^2 \quad (2.27)$$

where $J_{\text{max}} \approx (2\mu q\mu_D/\hbar^2)^{1/2}$ is independent of E. Equations 2.26 and 2.27, therefore, lead to

$$\langle J\rangle/J_{\text{max}} \approx 1/\sqrt{2} \approx 0.707 \quad (2.28)$$

Model valence potentials for atomic A and linear B combining to linear AB in ref 2 gave

$$\langle J\rangle/J_{\text{max}} \approx (1 - 1/\sqrt{2})^{1/2} \approx 0.541 \quad (2.29)$$

while the combination to T-shaped AB gave

$$\langle J\rangle/J_{\text{max}} \approx (1 - \sqrt{2/3})^{1/2} \approx 0.428 \quad (2.30)$$

Dipole−dipole systems treated in ref 2 led to

$$\langle J\rangle/J_{\text{max}} \approx 0.541 \quad (2.31)$$

Therefore, one may estimate $\langle J\rangle$ to be in the range

$$\langle J\rangle/J_{\text{max}} \approx 0.55 \pm 0.2 \quad (2.32)$$

Investigations with ab initio potentials are analyzed with respect to the ratio $\langle J\rangle/J_{\text{max}}$ in the following section.

The SACM/CT calculations from ref 2 illustrated that various types of J dependences of $f_{\text{rigid}}(E,J)$ can occur besides the dependence on $E - E_0(J)$. If the dynamics is nonadiabatic, i.e., has a small effective mass M and a Massey parameter $\xi = \sqrt{2M}$ smaller than unity, $f_{\text{rigid}}(E,J)$ tends to become independent of J/J_{max}. In this case our simple treatment with eqs 2.22−2.25 becomes fully adequate. In other cases with more complicated dependences of $f_{\text{rigid}}(E,J)$ on J, one may at least approximately reconstruct the J dependence around $\langle J\rangle$ by comparison with the model calculations from ref 2. The corresponding procedure is illustrated later on. It should be emphasized, however, that real systems can have quite specific properties where the present simple approach can only serve for a first estimate.

3. Practical Examples

The derived simple relationships between specific and thermal rigidity factors from section 2 provide opportunities for practical applications. To go beyond simple fitting of relatively undefined "activated complex frequencies" in conventional rigid activated complex RRKM theory, it requires realistic PST calculations of $k^{\text{PST}}(E,J)$ and $k_{\text{cap}}{}^{\text{PST}}(T)$. Unavoidably, this at first involves the determination of centrifugal barriers $E_0(J)$ with a realistic MEP potential $V(r)$ where r denotes the center-of-mass distance between A and B. In other words, for $J \approx L$, the centrifugal maxima $E_0(J)$ of the potential

$$V(r,J) = V(r) + J(J+1)\,\hbar^2/2\pi\mu r^2 \quad (3.1)$$

have to be calculated. Provided that one has $V(r)$ from ab initio or model calculations of the PES, this is an easy task. For instance, if the $C_8H_{10}{}^+$ system characterized in Figure 1 would be treated by an ion-induced dipole potential $V(r)$ only, one would have

$$V(r) \approx -\alpha\, q^2/2r \quad (3.2)$$

and $E_0(J)$ would be given by

$$E_0{}^{\text{ID}}(J) \approx [J(J+1)\,\hbar^2/2\mu]^2/2\alpha\, q^2 \quad (3.3)$$

Accounting for a short-range valence contribution to $V(r)$, in addition to the long-range ion-induced dipole part from eq 3.2, adds an additional factor to $E_0{}^{\text{ID}}(J)$ from eq 3.3. One obtains[5]

$$E_0(J) \approx E_0{}^{\text{ID}}(J)/(1 + 0.0169\,J + 2.65 \times 10^{-4}\,J^{1.79}) \quad (3.4)$$

Having determined $E_0(J)$, such as described for the $C_8H_{10}{}^+$ system, eqs 2.9 and 2.12 lead to $k_{\text{cap}}(T)$. The calculation of $k(E,J)$ is slightly more involved. It may be done with a standard rigid activated complex RRKM code. However, in this case the starting array of the Beyer−Swinehart state counting routine[8,9] for the conserved modes has to be chosen as $W(E,J)$ from section 2.2. On a simpler and often equally sufficient level, one may calculate $W(E,J)$ and $\rho(E,J)$ employing the Whitten−Rabinovitch formula[1,15] for the conserved modes and convolute this with $W(E,J)$ for the transitional modes from section 2.2.

3.1. Examples for Ionic Systems. We have recently treated a series of *n*-alkylbenzene cation systems[5,6] by SACM/CT calculations on model PESs, calibrating the leading anisotropy parameter of the potential by comparison with one experimental observable and then predicting all other quantities. These cases were characterized by small Massey parameters, i.e., by nonadiabatic dynamics, such that our method applies best, see above. In the following, we illustrate the results. We first again consider the reaction

$$C_8H_{10}{}^+ \leftrightarrow C_7H_7{}^+ + CH_3 \quad (3.5)$$

where $C_8H_{10}{}^+$ is the ethylbenzene and $C_7H_7{}^+$ the benzylium cation. Figure 1, such as obtained for this system,[5] indeed showed that $f_{\text{rigid}}(E,J)$ essentially only depends on $E - E_0(J)$,

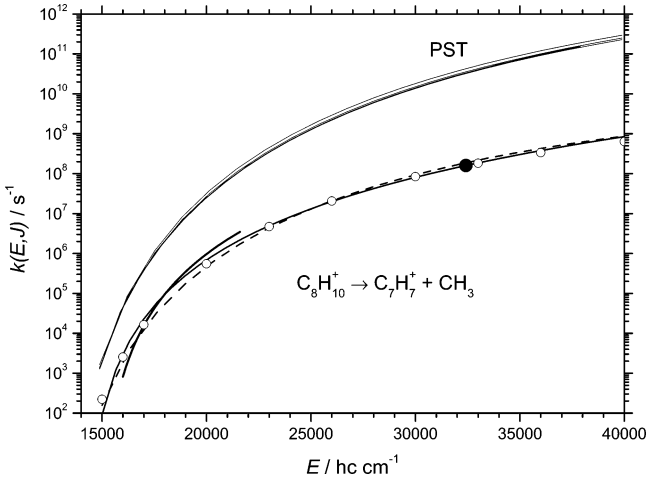

Figure 2. Specific rate constants $k(E,J)$ for the dissociation of $C_8H_{10}^+$ (see Figure 1; upper curves, PST with $J = 0$, 55, and 90 from bottom to top and $J = 0$ without centrifugal barriers (shorter curve); full line, empirical representation[18] of experimental $k(E)$ by $k(E) \propto (E\text{-}E_0)^{4.824}$, see ref 5; full circle, experimental result from ref 17; heavy line around 18000 cm^{-1}, experimental results from ref 16; dashed line, SACM/CT calculations of $k(E,J = 50)$; open circles, this work with $f_{rigid}(E,J)$ from eq 2.16 with the empirical fit parameter $T_0 = 376$ K).

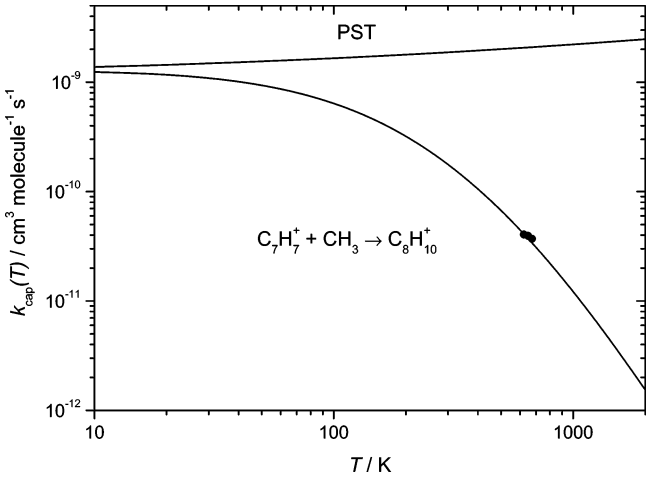

Figure 3. Thermal capture rate constants $k_{cap}(T)$ for the reaction $C_7H_7^+ + CH_3 \rightarrow C_8H_{10}^+$ (see Figures 1 and 2; upper curve, PST; lower curve, this work with $f_{rigid}(T) = [T_0/(T_0 + T)]^4$ and $T_0 = 376$ K, see eqs 2.18−2.20; points, experimental results from ref 19).

with $E_0(J)$ given by eqs 3.3 and 3.4. Approximating $f_{rigid}(E,J)$ from the detailed SACM/CT calculations illustrated in Figure 1 by eq 2.16 leads to the empirical fit parameter $T_0 = 376$ K. On the basis of this $f_{rigid}(E,J)$, our simplified approach to $k(E,J)$, e.g., gives a $k(E,J = 50)$ which in Figure 2 is compared with experimental[16,17] $k(E)$, with $k(E)$ from an empirical representation[18] in the form $k(E) \propto (E\text{-}E_0)^{s^*-1}$, with $k(E,J)^{PST}$ from PST, and with $k(E,J)$ from the detailed SACM/CT calculations.[5] The simple representation of $f_{rigid}(E,J)$ from Figure 1 by eq 2.22 performs very well indeed and well reproduces the experimental $k(E,J = 50)$ (E and $E_0(J)$ in our article are counted above the rovibrational ground state of separated A + B, where in contrast to this convention, E in $k(E)$ in the figures is always counted above the rovibrational ground state of the combined AB). Employing the derived parameters in eq 2.23 then leads to thermal capture rate constants such as shown in Figure 3. There is very good agreement between the limited available experiments[19]and the present simplified prediction of $k_{cap}(T)$ on the basis of the experimental data for $k(E)$. For this reaction system, experimental results have been obtained for specific rate

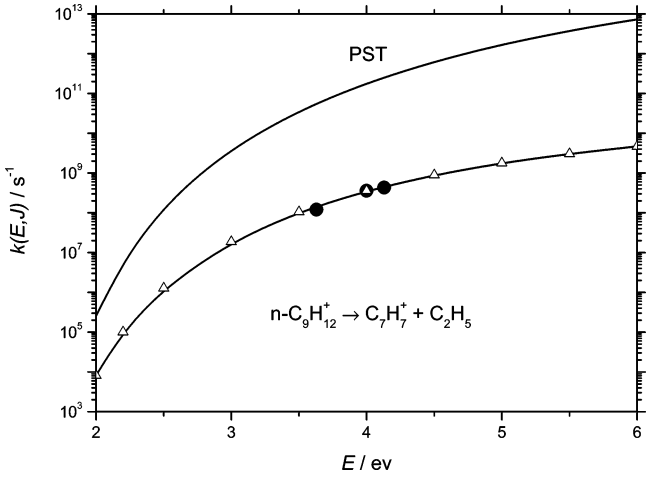

Figure 4. Specific rate constants $k(E,J)$ for the dissociation n-$C_9H_{12}^+ \rightarrow C_7H_7^+$ (benzylium) + C_2H_5 (upper curve, PST for $J = 50$; full circles, experimental results from ref 20; line through full circles, SACM/CT calculations for $J = 50$ from ref 5; open triangles, this work with $f_{rigid}(E,J = 50)$ from eq 2.16 with the empirical fit parameter $T_0 = 259$ K).

constants $k(E)$ and thermal rate constants. One of the two has been used to calibrate the anisotropy of the PES which then formed the basis of the SACM/CT calculations for the other quantity. As shown here, the described simple direct link between $k(E)$ and $k_{cap}(T)$ would have provided similarly good results and avoided the cumbersome SACM/CT calculations. However, one would have had to know in advance that one may use eq 2.16.

Measurements of $k(E)$[20] and $k_{cap}(T)$[21] have also been made for the dissociation of n-propylbenzene cations

$$n\text{-}C_9H_{12}^+ \Leftrightarrow C_7H_7^+ + C_2H_5 \qquad (3.6)$$

In this case, the experimental data for $k(E)$ were more fragmentary than for $C_8H_{10}^+$ but they also allowed $f_{rigid}(E,J)$ to be represented by eq 2.16 with the empirical fit parameter $T_0 = 259$ K. Figure 4 compares the derived simplified representation of $k(E,J = 50)$ with the experimental results[20] and SACM/CT calculations.[5] Good agreement between the two latter results are obtained. One should remember that the latter treatment also used the calibration of the anisotropy amplitude by the experimental $k(E)$. Employing eqs 2.16−2.21 for the link between $k(E,J)$ and $k_{cap}(T)$ leads to thermal capture rate constants such as illustrated in Figure 5. Again the experimental results[21] for $k_{cap}(T)$ are reproduced surprisingly well.

The dissociation of n-butylbenzene cations on the bond fission channel

$$n\text{-}C_{10}H_{14}^+ \rightarrow C_7H_7^+ + C_3H_7 \qquad (3.7)$$

has been studied experimentally in detail[22,23] with respect to the specific rate constants $k(E)$. The results can well be expressed by eq 2.22 with the empirical fit parameters $f_0 = 0.0037$, $f_1 = 1 - f_0$, and $T_1 = 179$ K. Similarly good agreement between this representation, SACM/CT calculations from ref 6, and the experiments has been found as for $C_8H_{10}^+$ and n-$C_9H_{12}^+$, such that we do not need to illustrate the data here. However, in this case, no measurements of $k_{cap}(T)$ have been made as yet. Although one predicts[24] that the competing tight transition state channel

$$n\text{-}C_{10}H_{14}^+ \rightarrow C_7H_8^+ + C_3H_6 \qquad (3.8)$$

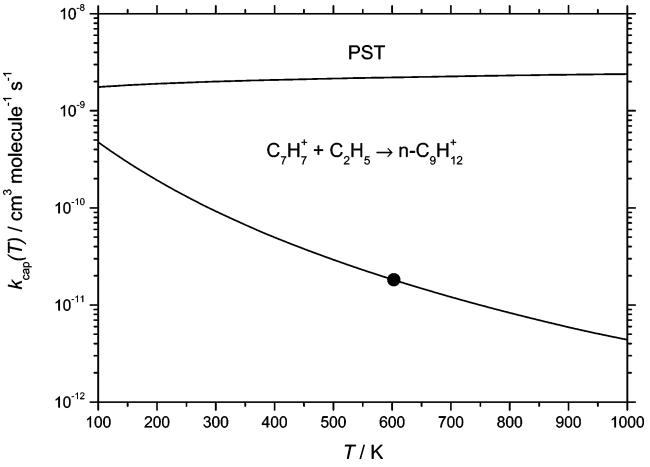

Figure 5. Thermal capture rate constants $k_{cap}(T)$ for $C_7H_7^+ + C_2H_5 \rightarrow$ *n*-$C_9H_{12}^+$ (upper curve, PST; full circle, experimental results from ref 21; line through experimental point, this work with $f_{rigid}(T) = [T_0/(T_0 + T)]^4$ from eqs 2.18−2.20 with $T_0 = 259$ K).

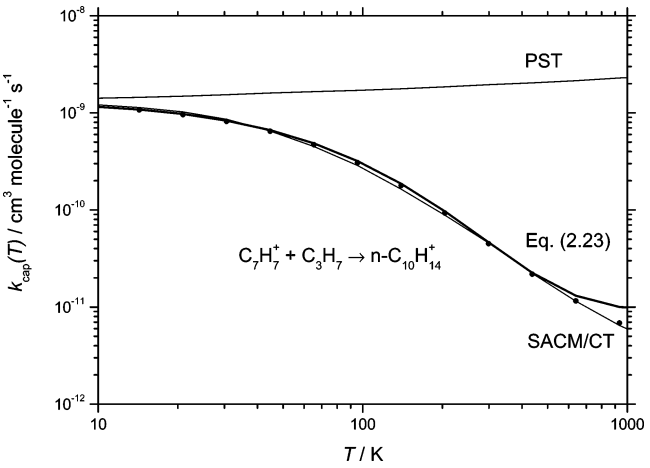

Figure 6. Thermal capture rate constants $k_{cap}(T)$ for $C_7H_7^+ + C_3H_7 \rightarrow$ *n*-$C_{10}H_{14}^+$ (upper curve, PST; lower curve without dots, SACM/CT calculations from ref 6 based on experimental results for $k(E)$ from refs 22 and 23; lower curve with dots, eq 2.23 with the empirical fit parameters $f_0 = 0.0037$, $f_1 = 1 - f_0$, $T_1 = 179$ K).

will dominate the thermal dissociation of *n*-$C_{10}H_{14}^+$ over wide temperature ranges, one may also be interested in the dissociation via channel 3.7 and the corresponding $k_{cap}(T)$ for the reverse association. Figure 6 shows the prediction by comparing the full SACM/CT modeling[6] with the simple link of $k_{cap}(T)$ and $k(E)$ by eq 2.23 using the parameters given above. Apart from a minor deviation at high temperatures, the agreement between the two methods to predict $k_{cap}(T)$ on the basis of the experimental $k(E)$ appears quite satisfactory.

There are two reasons why the simple procedure of eqs 2.14−2.25 works so well for the described *n*-alkylbenzene cations: on one hand, these systems have relatively strong isotropic long-range ion-induced dipole potentials; on the other hand, they are characterized by small Massey parameters ξ such that their dynamics is relatively nonadiabatic[2]. Both factors move $f_{rigid}(E,J)$ into the direction where there is no J dependence beyond that included in $E_0(J)$. As a consequence, one may use the functional form of $f_{rigid}(E,J)$ chosen in eqs 2.16 and 2.22.

In the following we now consider the $C_6H_6^+$ system and its dissociation

$$C_6H_6^+ \rightarrow C_6H_5^+ + H \qquad (3.9)$$

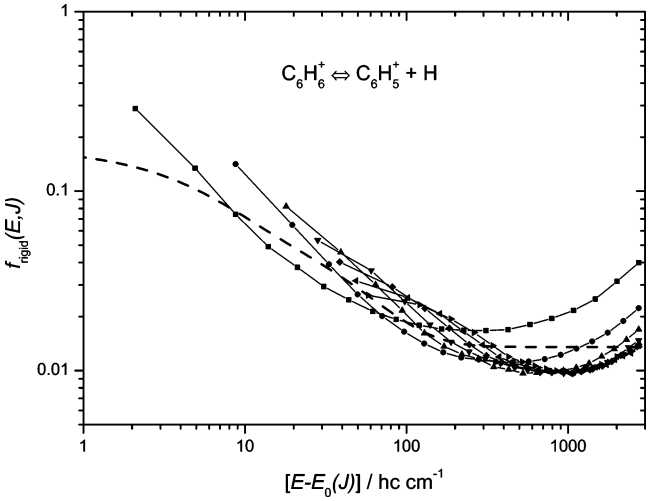

Figure 7. Specific rigidity factors $f_{rigid}(E,J)$ for the transitional modes in the dissociation of benzene cations $C_6H_6^+ \rightarrow C_6H_5^+ + H$ (curves with points, SACM/CT calculations from ref 6 for $J = 0$, 10, 20, 30, 40, 50 with starting points from left to right, reproducing experimental $k(E,J)$ from refs 25 and 26, see ref 6; dashed line, average curve $f_{rigid}(E,\langle J\rangle)$ reproducing $f_{rigid}(T)$).

which starts to behave in a different way. This system still has a small Massey parameter and, hence, it shows major deviations from adiabatic dynamics.[2,6] However, because of the small polarizability of H atoms, the isotropic long-range ion-induced dipole potential is so weak that the anisotropic short-range valence potential dominates. For the latter potential, there are large J dependences of $f_{rigid}(E,J)$ beyond those included in $E_0(J)$. These effects are more common in neutral systems such that the $C_6H_6^+$ system described in the following represents a transition case to systems considered in section 3.2.

To illustrate the transition character of the $C_6H_6^+$ system, we first look at SACM/CT calculations of $f_{rigid}(E,J)$ in Figure 7. Unlike Figure 1, which characterizes systems like $C_8H_{10}^+$, *n*-$C_9H_{12}^+$, and *n*-$C_{10}H_{14}^+$, there is a certain spread of the J-specific curves. The dashed line in the figure represents $f_{rigid}(E,\langle J\rangle)$ which, after thermal averaging, leads to $k_{cap}(T)$ such as derived by SACM/CT calculations. As the spread of the curves is only comparably small, for this case we do not elaborate the relation between $\langle J\rangle$ and J_{max} in detail but assume that eq 2.32 holds sufficiently well. More pronounced spreads of $f_{rigid}(E,J)$ will be analyzed in the following section 3.2. We note, however, that the experimental $k(E,J)$ from ref 25 and $k(E)$ from refs 25 and 26 are all very well reproduced by SACM/CT calculations[6] using a model PES which in part was based on ab initio calculations.[27]

Even though the measurements of $k(E)$ and of $k(E,J)$ in the $C_6H_6^+$ system are unusally detailed and accurate, it is important to emphasize that they are by far not sufficient to specify a complete $f_{rigid}(E,J)$ and a unique functional form of the type of eq 2.22 for $f_{rigid}(E,\langle J\rangle)$. In addition to the experiments, one requires knowledge of the character of the PES and SACM/CT calculations to find the adequate functional form for $f_{rigid}(E,J)$. In the present case, this was provided by the investigations from ref 6. The SACM/CT calculations of $f_{rigid}(T)$ led to results shown in Figure 8 which can be fitted by eq 2.23 up to the third term with the empirical fit parameters $n = 2.5$, $f_0 = 0.0135$, $f_1 = 0.109$, $f_2 = 0.0527$, $T_1 = 7.81$ K, and $T_2 = 58.6$ K. This expression then corresponds to the curve for $f_{rigid}(E,\langle J\rangle)$ shown in Figure 7. Employing centrifugal barriers $E_0(J)$ derived from the MEP of the PES and given by $E_0(J)/\text{hc cm}^{-1} \approx 1.88 \times 10^{-3}\, J^4/(1 + 0.114\, J^{1.3} + 0.0122\, J^2)$, one may also verify the

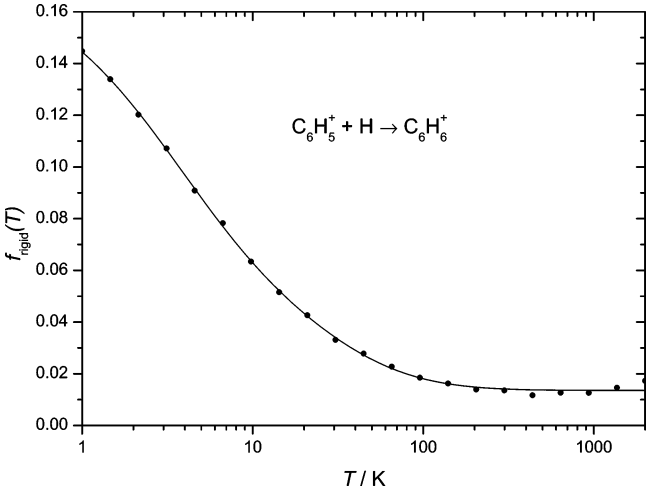

Figure 8. Thermal rigidity factor $f_{rigid}(T)$ for $C_6H_6^+ \leftrightarrow C_6H_5^+ + H$ (SACM/CT calculations from ref 6 such as illustrated in Figure 7).

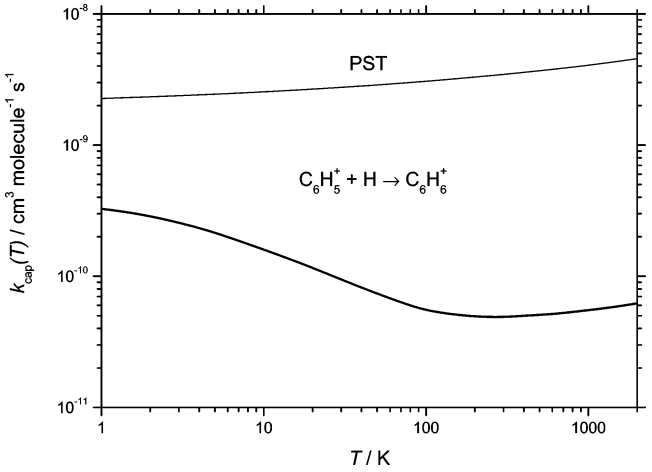

Figure 9. Thermal capture rate constants $k_{cap}(T)$ for $C_6H_5^+ + H \rightarrow C_6H_6^+$ (upper curve, PST; lower curve, $k_{cap}(T)$ corresponding to $f_{rigid}(T)$ from Figure 8 and the numerical representation given in the text).

validity of eq 2.31. Although the spread of the curves for $f_{rigid}(E,J)$ around the curve for $f_{rigid}(E,\langle J\rangle)$ is not large, eq 2.32 serves well for the estimate of $\langle J\rangle$. For instance, $f_{rigid}(E,\langle J\rangle)$ intersects with $f_{rigid}(E,J = 50)$ at $[E - E_0(J)]/hc \approx 340$ cm^{-1}. Having $E_0(\langle J\rangle = 50)/hc = 235$ cm^{-1} and $E_0(J_{max} = 74)/hc = 572$ cm^{-1} one obtains $\langle J\rangle/J_{max} \approx 0.68$ which is well within the limits of eq 2.31. For larger J, $f_{rigid}(E,J)$ becomes nearly J-independent and $f(E,\langle J\rangle)$ cannot be attributed to a specific $\langle J\rangle$ anymore. At the same time, the curve for $f_{rigid}(E,\langle J\rangle)$ in Figure 7 becomes relatively uncertain. The results of Figure 8 in Figure 9 are used to predict $k_{cap}(T)$. As in Figures 3, 5, and 6, $k_{cap}(T)$ at higher temperatures is far below $k_{cap}^{PST}(T)$. However, because of the much weaker long-range potential, the approach between $k_{cap}(T)$ and $k_{cap}^{PST}(T)$ takes place at much lower temperatures in $C_6H_6^+$ than in the alkylbenzene cations.

3.2. Examples for Neutral Systems. Specific rate constants $f_{rigid}(E,J)$ for the transitional modes may also show much stronger J dependences besides the dependence on $E - E_0(J)$ than shown in Figures 1 and 7. This will be the case, when the reaction approaches adiabatic dynamics with Massey parameters ξ larger than unity and when both the long-range and short-range parts of the potential are strongly anisotropic. As an example, we have chosen the H_2O_2 system

$$H_2O_2 \leftrightarrow 2HO \tag{3.10}$$

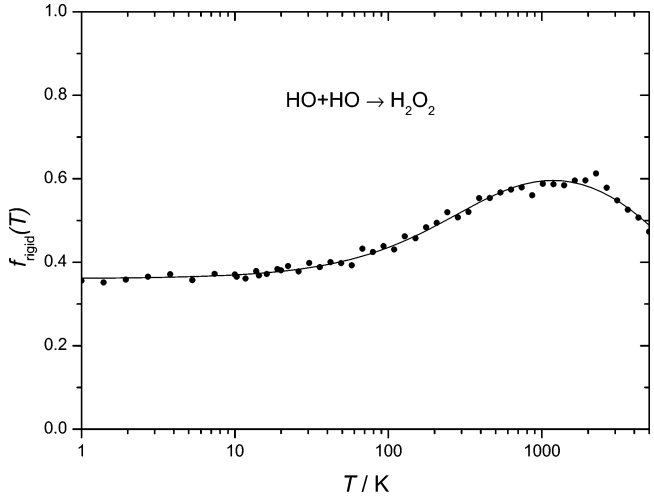

Figure 10. Thermal rigidity factor $f_{rigid}(T)$ for the reaction $H_2O_2 \leftrightarrow 2HO$ (filled circles, SACM/CT calculations from ref 4; full line, representation by eq 2.24 with parameters given in the text).

for which SACM/CT calculations have been made[4] on the ab initio PES from refs 28−30. The potential is characterized by strong long-range HO dipole−dipole and short-range H_2O_2 valence contributions. The relevant quantities $E_0(J)$, J_{max}, $f_{rigid}(E,J)$, and $f_{rigid}(T)$ for the dipole−dipole system have been derived explicitly in ref 2, being

$$E_0(J) = \{J(J+1)h^2/[6\mu(\mu_{D1}\mu_{D2})^{2/3}]\}^3 \tag{3.11}$$

$$J_{max}(J_{max}+1) = 6\mu E^{1/3}(\mu_{D1}\mu_{D2})^{2/3}/\hbar^2 \tag{3.12}$$

$$f_{rigid}(E,J) \approx [1 - (J/J_{max})^2]^3 \tag{3.13}$$

and

$$f_{rigid}(T) \approx 0.354 \tag{3.14}$$

where $\mu_{D1} = \mu_{D2} = \mu_D(HO)$ in this case. The combination of eqs 3.13 and 3.14 led to eq 2.31, see above. Considering the complete ab initio potential of H_2O_2, obviously one expects deviations from eqs 3.11−3.14. These are inspected in the following. Since the experimental data for $k(E,J)$ and $k_{cap}(T)$ are relatively fragmentary, see refs 31 and 32, in the following we rely on our SACM/CT calculations[4] on the ab initio potential and determine relationships between $f_{rigid}(E,J)$ and $f_{rigid}(T)$ by analyzing this theoretical modeling. We, nevertheless, note that the experimental data appear to be consistent with the SACM/CT results; see ref 4.

Thermal rigidity factors $f_{rigid}(T)$ for reaction 3.10 from the SACM/CT calculations are shown in Figure 10. One first notes that the thermal rigidity factor even for the real H_2O_2 system does not differ too much from the dipole−dipole value of 0.354. A fit to the form of eq 2.24 up to the third term again is possible such as shown in the figure. The empirical parameters of this fit are $n = 3$, $f_0 = 0.0413$, $f_1 = -0.320$, $f_2 = 0.639$, $T_1 = 1000$ K, and $T_2 = 40\,000$ K. By means of eq 2.22, specific rigidity factors $f_{rigid}(E,\langle J\rangle)$ are directly obtained such as shown in Figure 11. The comparison of this $f_{rigid}(E,\langle J\rangle)$ with $f_{rigid}(E,J)$ from the SACM/CT calculations[27] in Figure 11 indicates a very broad spread and, therefore, a strong J-dependence of $f_{rigid}(E,J)$ in addition to that on $E - E_0(J)$. The spread is much larger than in the $C_6H_6^+$ system illustrated in Figure 7 and is completely different from Figure 1, where it is absent. The broad spread of $f_{rigid}(E,J)$ around $f_{rigid}(E,\langle J\rangle)$ may suggest that there is no simple way from $f_{rigid}(T)$ to $f_{rigid}(E,J)$. However, this conclusion is not

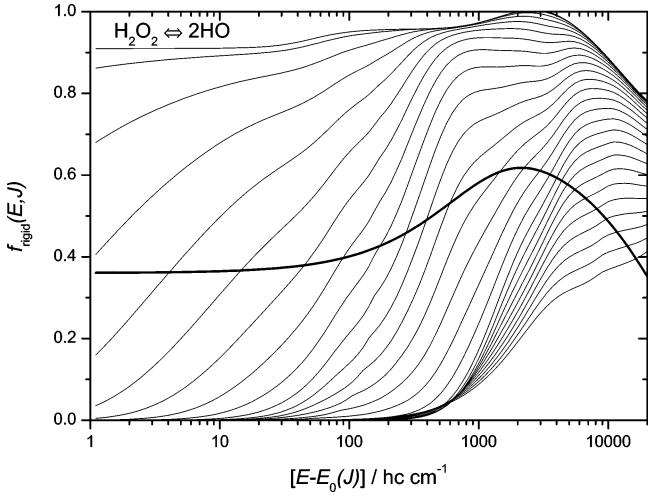

Figure 11. Specific rigidity factors $f_{rigid}(E,J)$ for the transitional modes in the reaction $H_2O_2 \leftrightarrow 2HO$ (set of light curves, SACM/CT calculations from ref 4 with $J = 1$ (top), 5, 10 ... 120, 125 (bottom); heavy curve, $f_{rigid}(E,\langle J\rangle)$ derived from $f_{rigid}(T)$, see Figure 10).

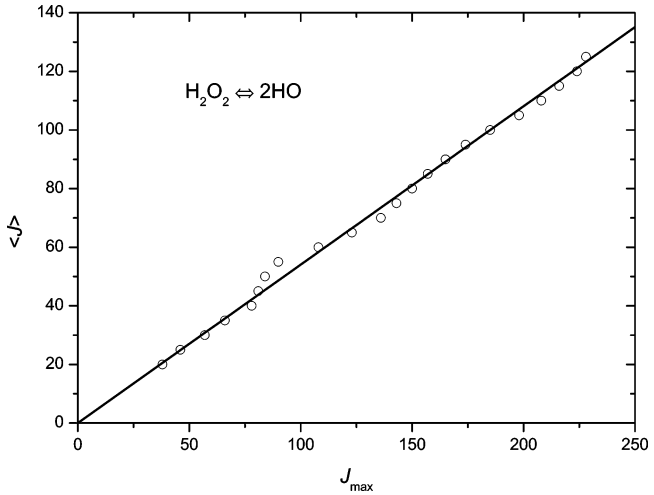

Figure 12. Average $\langle J\rangle$ as a function of $J_{max}(E)$ for $f_{rigid}(E,\langle J\rangle)$ in the reaction $H_2O_2 \leftrightarrow 2HO$ ($f_{rigid}(E,\langle J\rangle)$ derived from $f_{rigid}(T)$, see Figure 10; open circles, SACM/CT calculations from ref 4; full line, $\langle J\rangle = 0.541$ J_{max} like eq 2.31 for dipole−dipole potential).

right. First, there is a simple relation between $\langle J\rangle$ and J_{max}. Analyzing Figure 11 with respect to this relation, one obtains Figure 12 which is in perfect agreement with eq 2.31 for the pure dipole−dipole system. At a given energy E, therefore, $f_{rigid}(E,J)$ spreads between 0 and $J_{max}(E)$ around $\langle J\rangle$ such as given for the pure dipole−dipole system. Apparently, the specific rigidity factors of real H_2O_2 have the same general features as the dipole−dipole system. One then may try to reconstruct $f_{rigid}(E,J)$ from $f_{rigid}(E,\langle J\rangle)$ by scaling the dipole−dipole results from eq 3.13. Figure 13 demonstrates the success of the procedure which is described in the following.

By analogy to the dipole−dipole result of eq 3.13, we model $f_{rigid}(E,J)$ in the form

$$f_{rigid}(E,J) \approx [1 - (J/J_{max})^2]^n \qquad (3.15)$$

where the exponent n for each energy E is fitted in such a way that

$$f_{rigid}(E,\langle J\rangle) = [1 - (\langle J\rangle/J_{max})^2]^n \qquad (3.16)$$

where $\langle J\rangle/J_{max} = 0.541$ from eq 2.31 applies. Figure 13 shows

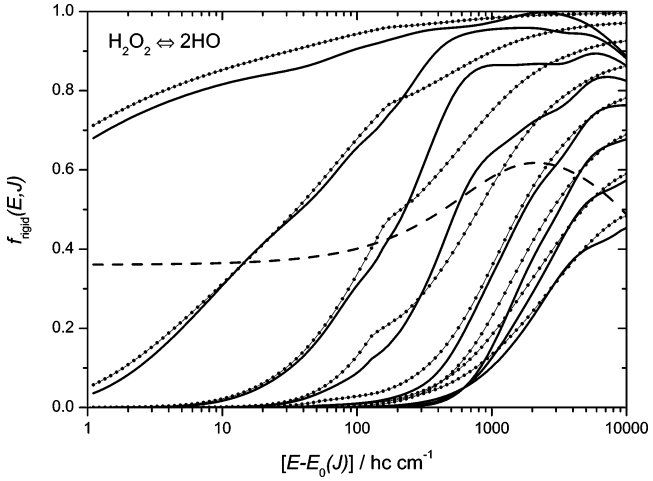

Figure 13. Reconstruction of $f_{rigid}(E,J)$ from $f_{rigid}(E,\langle J\rangle)$ in the reaction $H_2O_2 \leftrightarrow 2HO$ (dashed line, $f_{rigid}(E,\langle J\rangle)$ from Figure 11; full lines, SACM/CT calculations of $f_{rigid}(E,J)$ from ref 4, see Figure 11; lines with circles, reconstructed curves of $f_{rigid}(E,J)$ from $f_{rigid}(E,\langle J\rangle)$ and eqs 3.15 and 3.16 with $J = 15$, 30, 45, ..., 120 from top to bottom).

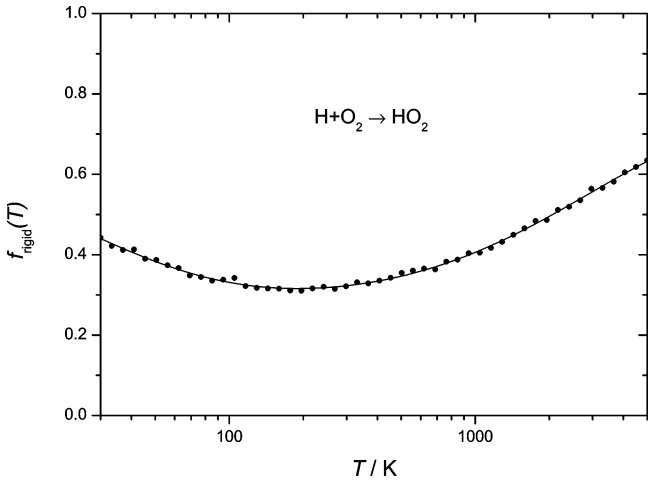

Figure 14. Thermal rigidity factors $f_{rigid}(T)$ for the reaction $H + O_2 \rightarrow HO_2$ (filled circles, SACM/CT calculations from ref 3; full line, fit by eqs 2.23−2.25 with the parameters given in the text).

that even with the complicated real PES of the H_2O_2 system the procedure works quite well and from $f_{rigid}(T)$, with the help of $J_{max}(E)$, allows one to construct a complete set of specific rigidity factors $f_{rigid}(E,J)$ for the transitional modes.

We have also analyzed the systems

$$HO_2 \leftrightarrow H + O_2 \qquad (3.17)$$

and

$$HO_2 \leftrightarrow HO + O \qquad (3.18)$$

in a way similar to the H_2O_2 system. Figures 14 and 15 illustrate reaction 3.17, Figures 16 and 17 are for reaction 3.18. $f_{rigid}(T)$ in Figure 14 is from SACM/CT calculations[3] on an ab initio potential which leads to good agreement with experimental results from ref 33. It can again be fitted in the form of eqs 2.23−2.25 with the empirical fit parameters $n = 2$, $f_0 = 0.782$, $f_1 = 0.425$, $f_2 = -0.519$, $T_1 = 52.1$ K, and $T_2 = 5820$ K, such that $f_{rigid}(E,\langle J\rangle)$ follows directly from eq 2.22. Figure 15 illustrates that there is again a considerable spread of $f_{rigid}(E,J)$ around this curve at small $E - E_0(J)$ while the spread diminishes at larger values. A reconstruction of the full $f_{rigid}(E,J)$ could be made with eqs 3.15 and 3.16 where $\langle J\rangle/J_{max} = 0.578$. Figure

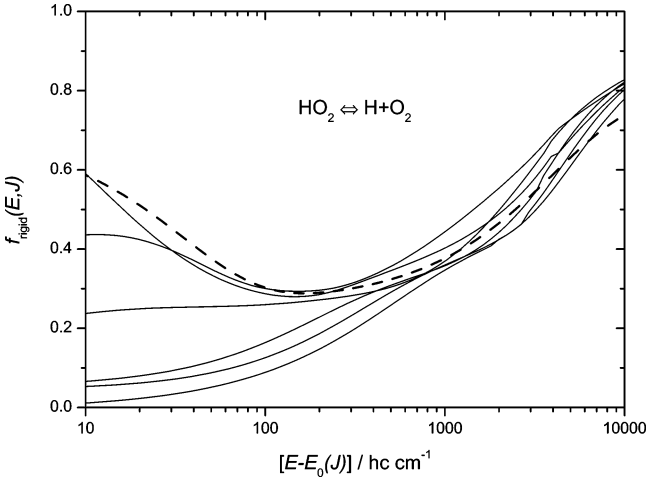

Figure 15. Specific rigidity factors $f_{rigid}(E,J)$ for the transitional modes in the reaction $HO_2 \leftrightarrow H + O_2$ (full lines, SACM/CT calculations from ref 3 for $J = 1$, 10, 20, 30, 40, and 50 from top to bottom; dashed line, $f_{rigid}(E,\langle J\rangle)$ derived from Figure 14).

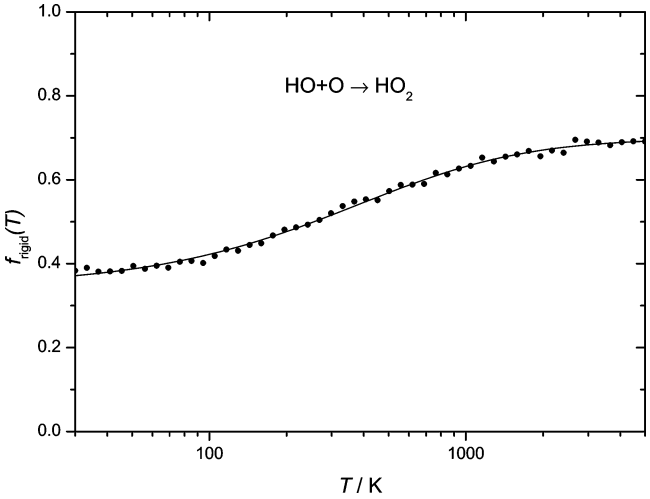

Figure 16. As for Figure 14, but for the process $HO + O \rightarrow HO_2$ (SACM/CT calculations from ref 34, fit with parameters given in the text).

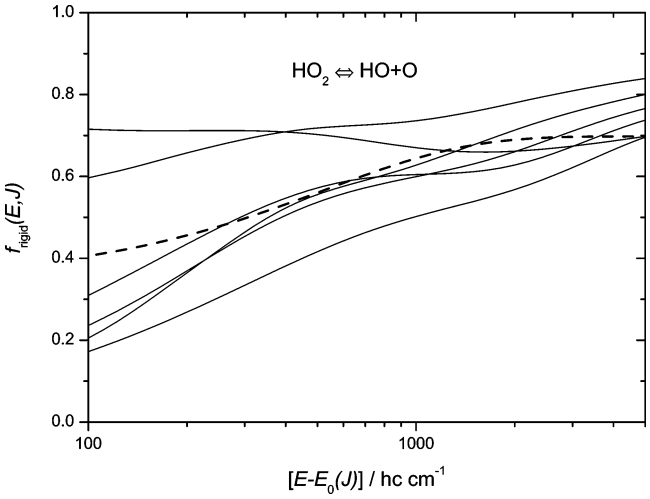

Figure 17. As for Figure 15, but for the process $HO_2 \leftrightarrow HO + O$ (full lines, SACM/CT calculations from ref 34 for $J = 1$ (top), 20, 40, 60, 80, 100 (bottom); dashed line, $f_{rigid}(E,\langle J\rangle)$ derived from Figure 16).

16 shows $f_{rigid}(T)$ for reaction 3.18 such as again calculated on an ab initio potential.[34] A fit in the form of eqs 2.23−2.25 with the empirical fit parameters $n = 2$, $f_0 = 0.698$, $f_1 = -0.353$, and $T_1 = 765$ K well reproduces the calculations. The corresponding $f_{rigid}(E,\langle J\rangle)$ from eq 2.22 in Figure 17 is compared with $f_{rigid}(E,J)$ which can be reconstructed also by eqs 3.15 and 3.16 with the same $\langle J\rangle/J_{max} = 0.578$ as used for reaction 3.17.

The given examples for neutral systems illustrate how $f_{rigid}(T)$ and $f_{rigid}(E,J)$ can be linked if there is a J dependence of $f_{rigid}(E,J)$ beyond that included in $E_0(J)$. The described procedure is by far less time-consuming than a full SACM/CT calculation on a complete PES.

4. Conclusions

We have analyzed the treatment of barrierless association and the reverse bond dissociation processes

$$A + B \leftrightarrow AB \tag{4.1}$$

from a practical point of view. Our approach in a first stage requires to do a phase-space theoretical calculation of thermal capture rate constants $k_{cap}(T)$ (or the corresponding high-pressure recombination or dissociation rate constants) and the corresponding specific rate constants $k(E)$ for dissociation of AB. This phase space theory should be done with the most realistic minimum energy path potential, either from ab initio or from model calculations for the potential of the transitional modes between A and B. These PST calculations cannot be avoided if any reasonable link between rate parameters and the potential is desired. In a second stage, the effects of the anisotropy of the potential are analyzed such as expressed by thermal rigidity factors $f_{rigid}(T)$ and specific rigidity factors $f_{rigid}(E,J)$ for the transitional modes. Our approach can take advantage of theoretical calculations, such as SACM/CT calculations, or it works without them when they are not available. In the latter case it employs experimental data only, on the level as they are available, and it provides estimates for the complementary rigidity factors. For instance, if thermal capture rate constants $k_{cap}(T)$ are available at a single temperature or over a certain temperature range, it provides specific rigidity factors for the calculation of specific rate constants $k(E)$ at a single energy or over a certain energy range. In addition, it allows one to approximately construct specific rigidity factors $f_{rigid}(E,J)$ for the complete determination of $k(E,J)$. If, on the other hand, specific rate constants for dissociation $k(E)$ are available, it leads to the corresponding thermally averaged analogues $k_{cap}(T)$. We have demonstrated our method both for ionic and for neutral reaction systems. These two classes of reactions have much in common and can be represented by one unifying approach. Differences are not found so much between ionic and neutral reactions but between reactions which are dominated by differing relative magnitudes of the short-range and long-range contributions of the potentials. The long-range contributions are generally more important in the class of ionic reactions but the opposite may also be found in some cases. We hope that the method outlined in this article because of its simplicity and versatility will find wide practical applications.

Acknowledgment. We thank Professor David Golden for many fruitful discussions on the present topic. His hindrance parameters are related to our rigidity factors in an intricate way. We also thank Albert Viggiano for helpful suggestions. Financial support for this work within the AFOSR Award No. FA8655-03-1-3034 as well as by the Deutsche Forschungsgemeinschaft (SFB 357 "Molekulare Mechanismen unimolekularer Prozesse") is also gratefully acknowledged.

References and Notes

(1) Baer, T.; Hase, W. L. *Unimolecular Reaction Dynamics. Theory and Experiments*; Oxford University Press: New York and Oxford, U.K., 1996).

(2) Maergoiz, A. I.; Nikitin, E. E.; Troe, J.; Ushakov, V. G. *J. Chem. Phys.* **2002**, *117*, 4201.

(3) Harding, L. B.; Troe, J.; Ushakov, V. G. *Phys. Chem. Chem. Phys.* **2000**, *2*, 631.

(4) Troe, J.; Ushakov, V. G. *Phys. Chem. Chem. Phys.*, submitted.

(5) Troe, J.; Ushakov, V. G.; Viggiano, A. A. *Z. Phys. Chem.* **2005**, *219*, 715.

(6) Troe, J.; Ushakov, V. G.; Viggiano, A. A. *J. Phys. Chem. A*, submitted.

(7) Troe, J. *J. Chem. Phys.* **1981**, *75*, 226. Cobos, C. J.; Troe, J. *J. Chem. Phys.* **1985**, *83*, 1010.

(8) Beyer, T.; Swinehart, D. F. *Commun. Assoc. Comput. Mach.* **1973**, *16*, 379. Stein, S. E.; Rabinovitch, B. S. *J. Chem. Phys.* **1973**, *58*, 2438.

(9) Astholz, D. C.; Troe, J.; Wieters, W. *J. Chem. Phys.* **1979**, *70*, 5107 (Appendix A).

(10) Chesnavich, W. J.; Bowers, M. T. In *Gas-Phase Ion Chemistry*; Bowers, M. T., Ed.; Academic Press: New York, 1979; Vol. 1, p 119.

(11) Troe, J. *J. Chem. Phys.* **1983**, *79*, 6017 (Appendix A and C, $W_1(E,J)$ from this reference in the absence of centrifugal barriers corresponds to the present $W_0(E,J)$).

(12) Olzmann, M.; Troe, J. *Ber. Bunsen-Ges. Phys. Chem.* **1992**, *96*, 1327. Olzmann, M.; Troe, J. *Ber. Bunsen-Ges. Phys. Chem.* **1994**, *98*, 1563 (see ref 11 therein).

(13) Klots, C. E.; Polach, J. *J. Phys. Chem.* **1995**, *99*, 15396.

(14) Troe, J. *J. Phys. Chem.* **1979**, *83*, 114.

(15) Forst, W. *Theory of Unimolecular Reactions*; Academic Press: New York and London, 1973).

(16) Malow, M.; Penno, M.; Weitzel, K.-M. *J. Phys. Chem. A* **2003**, *107*, 10625.

(17) Kim, Y. H.; Choe, J. C.; Kim, M. S. *J. Phys. Chem. A* **2001**, *105*, 5751.

(18) Troe, J. *J. Phys. Chem.* **1983**, *87*, 1800.

(19) Fernandez, A. I.; Viggiano, A. A.; Maergoiz, A. I.; Troe, J.; Ushakov, V. G. *Int. J. Mass Spectrom.* **2005**, *241*, 305.

(20) Hwang, W. G.; Moon, J. H.; Choe, J. C.; Kim, M. S. *J. Phys. Chem. A* **1998**, *102*, 7512.

(21) Fernandez, A. I.; Viggiano, A. A.; Miller, Th. M.; Williams, S.; Troe, J. *J. Phys. Chem. A* **2004**, *108*, 9652.

(22) Baer, T.; Dutuit, O.; Mestdagh, H.; Rolando, C. *J. Phys. Chem.* **1988**, *92*, 5674.

(23) Oh, S. T.; Choe, J. C.; Kim, M. S. *J. Phys. Chem.* **1996**, *100*, 13367.

(24) Fernandez, A. I.; Viggiano, A. A.; Troe, J. *J. Phys. Chem. A*, submitted.

(25) Kiermeier, A.; Kühlewind, H.; Neusser, H. J.; Schlag, E. W.; Lin, S. *J. Chem. Phys.* **1988**, *88*, 6182.

(26) Klippenstein, S. J.; Faulk, J. D.; Dunbar, R. C. *J. Chem. Phys.* **1993**, *98*, 243.

(27) Klippenstein, S. J. *Int. J. Mass Spectrom. Ion Processes* **1997**, *167/168*, 235.

(28) Kuhn, B.; Rizzo, T. R.; Luckhaus, D.; Quack, M.; Suhm, M. A. *J. Chem. Phys.* **1999**, *111*, 2565.

(29) Harding, L. B. *J. Phys. Chem.* **1989**, *93*, 8004; **1991**, *95*, 8653.

(30) Koput, J.; Carter, S. C.; Handy, N. C. *J. Phys. Chem. A* **1998**, *102*, 6325; *J. Chem. Phys.* **2001**, *115*, 8345.

(31) Brouwer, L.; Cobos, C. J.; Troe, J.; Dübal, H.-R.; Crim, F. F. *J. Chem. Phys.* **1987**, *86*, 6171.

(32) Fulle, D.; Hamann, H. F.; Hippler, H.; Troe, J. *J. Chem. Phys.* **1996**, *105*, 1001.

(33) Hahn, J.; Krasnoperov, L.; Luther, K.; Troe, J. *Phys. Chem. Chem. Phys.* **2004**, *6*, 1997.

(34) Harding, L. B.; Maergoiz, A. I.; Troe, J.; Ushakov, V. G. *J. Chem. Phys.* **2000**, *113*, 11019.